JPET Fast Forward. Published on January 29, 2016 as DOI: 10.1124/jpet.115.230565
This article has not been copyedited and formatted. The final version may differ from this version.

Systems pharmacology analysis of the amyloid cascade following β-secretase inhibition enables the identification of an Aβ42 oligomer pool

Eline M.T. van Maanen Tamara J. van Steeg Maria S. Michener
Mary J. Savage Matthew E. Kennedy Huub Jan Kleijn
Julie A. Stone Meindert Danhof

Division of Pharmacology Leiden Academic Center for Drug Research, Leiden University, Leiden, The Netherlands (E.M., M.D.); Leiden Experts on Advanced Pharmacokinetics & Pharmacodynamics, Leiden, The Netherlands (E.M., T.S.); Merck Research Laboratories, Whitehouse Station, NJ (M.M., M.S., M.K., H.K., J.S.)

Downloaded from jpet.aspetjournals.org at ASPET Journals on April 10, 2024

JPET Fast Forward. Published on January 29, 2016 as DOI: 10.1124/jpet.115.230565
This article has not been copyedited and formatted. The final version may differ from this version.

Running title: Systems pharmacology analysis of the amyloid cascade

Corresponding author: Meindert Danhof
Corresponding author's address: Leiden University Gorlaeus Laboratories
Einsteinweg 55, P.O. Box 9502, 2300 RA Leiden
The Netherlands
Corresponding author's phone: +31-71-5276215
Corresponding author's fax: +31-71-5276292
Corresponding author's email: m.danhof@lacdr.leidenuniv.nl

# of text pages:	23
# of tables:	2
# of figures:	7
# of references:	43
Abstract word count:	213
Introduction word count:	760
Discussion word count:	1805

Recommended section assignment: Neuropharmacology

Downloaded from jpet.aspetjournals.org at ASPET Journals on April 10, 2024

JPET Fast Forward. Published on January 29, 2016 as DOI: 10.1124/jpet.115.230565
This article has not been copyedited and formatted. The final version may differ from this version.

Abbreviations:

Aβ	amyloid-β
Aβ_{O}	amyloid-β oligomer
AD	Alzheimer's disease
APP	β-amyloid precursor protein
BACE1	β-secretase
BACEi	β-secretase inhibitor
CI	confidence interval
CMP	cisterna magna ported
CSF	cerebrospinal fluid
C_{target}	drug concentration target site
C99	C-terminal membrane-bound 99-amino acid fragment
ELISA	enzyme-linked immunosorbent assay
IC_{50}	median inhibition concentration
LC-MS/MS	liquid chromatography tandem mass spectrometry
Kin_{40}	Aβ40 formation rate
Kin_{42}	Aβ42 formation rate
Kout	Aβ degradation rate
Kpl	oligomerization rate
KtAB	transit rate Aβ from brain to CSF
KtAP	transit rate sAPPα and sAPPβ from brain to CSF
Krev	Aβ_{O} dissociation rate
MTT	mean transit time
PK	pharmacokinetic
PD	pharmacodynamic
RinAPP	zero order input constant for APP
Rinα	sAPPα formation rate
Rinβ	sAPPβ formation rate
Rout	sAPPβ degradation rate
Routa	sAPPα degradation
sAPPα	soluble APP alpha
sAPPβ	soluble APP beta

Downloaded from jpet.aspetjournals.org at ASPET Journals on April 10, 2024

JPET Fast Forward. Published on January 29, 2016 as DOI: 10.1124/jpet.115.230565
This article has not been copyedited and formatted. The final version may differ from this version.

Abstract

The deposition of amyloid-β oligomers in brain parenchyma has been implicated in the pathophysiology of Alzheimer's disease. Here we present a systems pharmacology model describing the changes in the amyloid precursor protein (APP) pathway following administration of three different doses (10, 30 and 125 mg/kg) of the β-secretase (BACE1) inhibitor MBi-5 in cisterna magna ported rhesus monkeys. The time course of the MBi-5 concentration in plasma and cerebrospinal fluid (CSF) was analyzed in conjunction with the effect on the concentrations of the APP metabolites Aβ42, Aβ40, sAPPα and sAPPβ in CSF. The systems pharmacology model contained expressions to describe the production, elimination and brain-to-CSF transport for the APP metabolites. Upon the administration of MBi-5 a dose dependent increase of the metabolite sAPPα and dose dependent decreases of sAPPβ and Aβ were observed. Maximal inhibition of BACE1 was close to 100% and the value of the IC_{50} was 0.0256 μM (95% CI, 0.0137-0.0375). A differential effect of BACE1 inhibition on Aβ40 and Aβ42 was observed, with the Aβ40 response being larger than the Aβ42 response. This enabled the identification of an Aβ42 oligomer pool in the systems pharmacology model. These findings indicate that decreases in monomeric Aβ responses resulting from BACE1 inhibition are partially compensated by dissociation of Aβ oligomers and suggest that BACE1 inhibition may also reduce the putatively neurotoxic oligomer pool.

Downloaded from jpet.aspetjournals.org at ASPET Journals on April 10, 2024

JPET Fast Forward. Published on January 29, 2016 as DOI: 10.1124/jpet.115.230565
This article has not been copyedited and formatted. The final version may differ from this version.

Introduction

The amyloid cascade hypothesis posits that amyloid-β protein (Aβ) peptide levels are increased early in Alzheimer's disease (AD) leading to the formation of toxic soluble Aβ oligomers (Aβ_{O}) and plaques (Di Carlo et al., 2012). According to this hypothesis, a series of causal events initiated by abnormal Aβ levels leads to neuronal cell death and cognitive and functional decline over time (Hardy and Selkoe, 2002). Toxic Aβ_{O} are considered to be the drivers of the neurodegeneration (Benilova et al., 2012; Klein, 2013). Such soluble forms of multimeric Aβ peptides are intermediate of soluble Aβ monomers and insoluble Aβ fibrils and likely consist of a mixture of oligomeric species. Aβ dimers, trimers, larger Aβ_{O} and structures such as soluble protofibrils have been isolated from AD brain (Savage et al., 2014; Esparza et al., 2013; Mc Donald et al., 2010; Yang et al., 2013). Aβ_{O} are in a constant equilibrium with Aβ monomers and other Aβ aggregates (Benilova et al., 2012).

Formation of Aβ requires proteolytic cleavage of the transmembrane protein 'β-amyloid precursor protein' (APP). Sequential cleavage of APP by the enzymes β-secretase (BACE1) and γ-secretase leads to the formation of Aβ (Esler and Wolfe, 2001), as schematically depicted in Fig. 1. Here cleavage by BACE1 leads to the formation of both the N-terminal secreted fragment soluble APPβ (sAPPβ) and the C-terminal membrane-bound 99-amino acid fragment (C99). C99 is subsequent subject to cleavage by γ-secretase yielding Aβ species of different chain length. The most common Aβ isoforms have 38 (Aβ38), 40 (Aβ40) or 42 (Aβ42) amino acids (Wiltfang et al., 2002). In parallel full length APP is also cleaved by α-secretase leading to the formation of soluble APPα (sAPPα), which is non-amyloidogenic (Portelius et al., 2011).

Aβ production in brain is a target for AD therapy, with the potential for a disease modifying effect by reducing Aβ levels (Husain et al., 2008). Several BACE1 inhibitors (BACEi) are being tested in human clinical trials, but the optimum level of BACE1 inhibition required for the treatment of AD remains to be determined (Yan and Vassar, 2014). A quantitative understanding of the effects of secretase inhibitors on the APP pathway may provide greater insights into

Downloaded from jpet.aspetjournals.org at ASPET Journals on April 10, 2024

JPET Fast Forward. Published on January 29, 2016 as DOI: 10.1124/jpet.115.230565
This article has not been copyedited and formatted. The final version may differ from this version.

dose-response pharmacology relationships.

Generally, measures of Aβ response in humans and primates can only be obtained in CSF and not in brain. However, it is believed that changes in Aβ concentrations in CSF reflect changes in brain Aβ (Lu et al., 2012). Thus, CSF Aβ serves as key biomarker for Aβ production targeted therapies (Jack and Holtzman, 2013). The cisterna magna ported (CMP) rhesus monkey model enables longitudinal sampling in the CSF outflow from the cisterna magna in conscious rhesus. As APP is completely homologous between human and rhesus, the CMP rhesus monkey model is used to study the effects of secretase inhibitors (Podlisny et al., 1991; Gilberto et al., 2003; Cook et al., 2010).

Several studies on the pharmacokinetics (PK) and the pharmacodynamics (PD) of BACE1 and γ-secretase inhibitors have been reported (Lu et al., 2013, 2012; Janson et al., 2014; Parkinson et al., 2013). Liu et al. (2013) proposed a mechanistic PK-PD model of BACE1 inhibition in monkeys. They identified the β-secretase cleavage step as the rate limiting step for Aβ formation. However, their model is a simplification of the underlying system as no distinction is made between the β-secretase and γ-secretase cleavage steps and Aβ was modeled as a direct product of APP. Potter et al. (2013) used compartmental modeling to investigate the APP processing pathway based on the results from a metabolic tracer study in humans with rare autosomal dominant AD (ADAD). A model with 18 compartments accounting for the kinetics of Aβ38, Aβ40 and Aβ42 enrichments, including compartments representing APP and C99 was proposed. However, the reported model is structurally and numerically unidentifiable, considering that not all APP metabolites were measured.

No systems pharmacology model has been reported that provides an integrated description of the effects of drugs on the APP metabolites. Systems pharmacology modeling is an extension of traditional mechanism-based PK-PD modeling, linking the system that is affected by the drug to its treatment associated measured biomarkers. This involves computational analysis of the time course of the changes in biomarkers on the basis of a structural mathematical model that

Downloaded from jpet.aspetjournals.org at ASPET Journals on April 10, 2024

JPET Fast Forward. Published on January 29, 2016 as DOI: 10.1124/jpet.115.230565
This article has not been copyedited and formatted. The final version may differ from this version.

describes the underlying biological processes, while making a strict distinction between drug-specific and systems specific parameters. It has been demonstrated that such mechanism-based PK-PD models have much improved properties for extrapolation and prediction (Danhof et al., 2005, 2007). Systems pharmacology modeling will provide a quantitative understanding of the effects of drugs on the APP processing pathway to improve the prediction and magnitude of Aβ reducing effects.

The objective of this investigation was to characterize the multi-step production of Aβ in brain and its disposition into CSF in rhesus and obtain an indirect impression of Aβ_{O} using information from the monomeric Aβ species. To this end, CSF Aβ dynamic data from CMP monkeys treated with the BACEi MBi-5 were analyzed. APP metabolites inter-relationships and their responses to MBi-5 were each measured by ELISA and metabolite responses were then integrated by means of a systems pharmacology modeling approach. Comprehensive, model-based information from MBi-5 PK and PD is integrated across time points, doses and endpoints, yielding information on dose response and APP metabolite (sAPPβ, sAPPα and Aβ) responses and interrelationships. In this manner invaluable information is obtained on the functioning of the integrated biological system. The effect of BACE1 inhibition on Aβ_{O} is anticipated which will be measured in future studies.

Downloaded from jpet.aspetjournals.org at ASPET Journals on April 10, 2024

JPET Fast Forward. Published on January 29, 2016 as DOI: 10.1124/jpet.115.230565
This article has not been copyedited and formatted. The final version may differ from this version.

Materials and Methods

Animals

Animal use procedures were conform to the Guide for the Care and Use of Laboratory Animals (Institute of Laboratory Animal Resources, National Research Council, 1996) and reviewed and approved by the Institutional Animal Care and Use Committee at Merck Research Laboratories. The CMP rhesus monkey model was described by (Gilberto et al., 2003). The rhesus monkeys are chronically implanted with catheters in the cisterna magna, allowing repeated sampling of CSF and plasma in conscious rhesus. Six male animals, weighing between 5.2 and 11.7 kg (average, 8.7 kg), age 2 to 10 years (average, 8 years), were included in the study. These monkeys were captive-bred in a closed colony and individually housed.

Drug administration and sampling

The study protocol and pharmacological profile of MBi-5 was described previously by (Dobrowolska et al., 2014a). The study protocol is summarized here. In a single dose, four-way, full crossover study, MBi-5 was administrated at 10, 30, 125 mg/kg (5 ml/kg), or vehicle (0.4% methylcellulose) p.o., with at least two weeks washout between each period. Plasma and CSF drug concentrations were collected at 0 (predose) and 3, 5, 7, 9, 13, 16, 19, 22, 25, 28, 31, 49, 55, 58, 73 and 145 h postdose, resulting in 17 plasma and CSF PK samples for each monkey per treatment group. 2 mL of blood and 1 mL of CSF were collected at each time point. The concentration of MBi-5 in the plasma and CSF samples was determined using LC-MS/MS.

The concentrations of Aβ40, Aβ42, sAPPα and sAPPβ were determined from CSF samples collected at -22, -20 and -1 h (predose) and 2, 4, 6, 8, 12, 15, 18, 21, 24, 27, 30, 48, 54, 57, 72 and 144 h postdose, giving 19 measurements of each biomarker for each monkey per treatment group. 1 mL of CSF were collected at each time point. The assays used for the concentration measurements were described previously (Wu et al., 2011; Sankaranarayanan et al., 2009).

Downloaded from jpet.aspetjournals.org at ASPET Journals on April 10, 2024

JPET Fast Forward. Published on January 29, 2016 as DOI: 10.1124/jpet.115.230565
This article has not been copyedited and formatted. The final version may differ from this version.

PK-PD analysis

The PK-PD model was developed and fitted to the data by means of non-linear mixed effects modeling using the NONMEM software package version VI level 2 (Beal, 2008). This approach takes into account structural (fixed) effects and both intra- and interindividual variability. The following parameters are estimated: typical values of structural model parameters (population parameters, which define the average value for a parameter in a population) (θ), the variance and covariance of the interindividual variability (ω^2) and the variance of the residual error (σ^2). A step-wise procedure was used to find the model that best fitted the data. A convergence criterion of three significant digits in the parameter estimates was used. The obtained minimum value of the objective function was used for the comparison of nested models. A decrease of 10.8 points in the minimum value of the objective function by adding an additional parameter, corresponding to $p<0.001$ in a χ-squared distribution, was considered significant. The first-order conditional estimation approximation with η-ϵ interaction (FOCE interaction) was used for parameter estimation. Random effects at the individual level were included as exponential (e^{η}), reflecting lognormal distributions of the individual model parameters:

$$\theta_i = \theta \times e^{(\eta_i)} \tag{1}$$

in which θ_{i} is the value for the i^{th} individual; θ is the typical value for the parameter, and η is an interindividual random effect, which is assumed to follow a normal distribution with mean zero and variance ω^2.

The residual variability was explored with additive (Eq. 2) and proportional (Eq. 3) error

Downloaded from jpet.aspetjournals.org at ASPET Journals on April 10, 2024

JPET Fast Forward. Published on January 29, 2016 as DOI: 10.1124/jpet.115.230565
This article has not been copyedited and formatted. The final version may differ from this version.

models or a combination of both (Eq. 4) .

$$y_{ijk} = f(\theta_{ij}) + \epsilon_{ijk} \tag{2}$$

$$y_{ijk} = f(\theta_{ij}) \times (1 + \epsilon_{ijk}) \tag{3}$$

$$y_{ijk} = f(\theta_{ij}) \times (1 + \epsilon_{ijk1}) + \epsilon_{ijk2} \tag{4}$$

where y_{ijk} is the k^{th} observation on the j^{th} occasion for the i^{th} individual; $f(\theta_{ij})$ is the corresponding model predicted observation and ϵ represents the residual departure of the observed concentration from the predicted concentration, which is assumed to follow a normal distribution with mean zero and variance σ^2.

To evaluate the prediction of the central tendency and distribution of the observed data by the model a visual predictive check (VPC) was performed in which the median and the 90% inter-quantile range of the data simulated with the developed model were plotted together with the observations. A validated result would have close agreement of median observed and predicted line with ∼90% of the observations falling within the 90% prediction interval.

The NONMEM software package was implemented on an Intel QuadCore (Intel® Core™ i7 CPU860, 2.80 GHz, 3.24 GB RAM) and Compaq Visual Fortran (version 6.6, Compaq Computer Corporation, Houston, Texas, USA) was used as compiler. Data management and model assessment was done using the statistical software package S-PLUS for Windows (version 8.0 Professional, Insightful Corp., Seattle, USA).

Model description

The systems pharmacology model of MBi-5 was developed by sequential analysis of PK and PD data. The PK model of MBi-5 was based on simultaneous analysis of plasma and CSF PK data. The results of the PK data analysis is provided in the Supplemental Material. The PK profiles of MBi-5 observed in plasma and CSF were adequately described (Supplemental Figure 2), thus

Downloaded from jpet.aspetjournals.org at ASPET Journals on April 10, 2024

JPET Fast Forward. Published on January 29, 2016 as DOI: 10.1124/jpet.115.230565
This article has not been copyedited and formatted. The final version may differ from this version.

the model could serve as input for PD model analysis.

The biomarker response profiles of MBi-5 measured in CSF were adequately described by a model containing compartments for five variables: APP, sAPPβ, sAPPα, Aβ40 and Aβ42 (Fig. 2). The production of APP was believed to be zero order, i.e. a constant production of APP. It was assumed that there is no alternative proteolytic enzyme cleaving full length APP other than α-secretase and BACE1. As both sAPPβ and C99 are products of APP cleavage by BACE1, sAPPβ and C99 were presumed to follow the same kinetics and therefore sAPPβ could be used in the model as surrogate precursor for Aβ. The production of sAPPα, sAPPβ and Aβ were assumed to be first order, i.e. dependent on the concentration of its precursor. The interaction between APP, sAPPβ, sAPPα, Aβ40 and Aβ42 is described by Eqs. 5 - Eqs. 9:

$$\frac{d}{dt}APP = Rin_{APP} - (Rin\beta \times EFF + Rin\alpha) \times APP \tag{5}$$

$$\frac{d}{dt}sAPP\alpha = Rin\alpha \times APP - Rout_a \times sAPP\alpha \tag{6}$$

$$\frac{d}{dt}sAPP\beta = Rin\beta \times EFF \times APP - (Kin_{40} + Kin_{42}) \times sAPP\beta \tag{7}$$

$$\frac{d}{dt}A\beta_{40} = Kin_{40} \times sAPP\beta - Kout \times A\beta_{40} \tag{8}$$

$$\frac{d}{dt}A\beta_{42} = Kin_{42} \times sAPP\beta - Kout \times A\beta_{42} \tag{9}$$

The rate of change of APP with respect to time in the presence of the inhibitor is described by Eqs. 5, in which the BACE1 cleavage inhibition is incorporated by the factor *EFF*. *EFF* is the

Downloaded from jpet.aspetjournals.org at ASPET Journals on April 10, 2024

JPET Fast Forward. Published on January 29, 2016 as DOI: 10.1124/jpet.115.230565
This article has not been copyedited and formatted. The final version may differ from this version.

degree of inhibition caused by MBi-5, expressed as shown in Eqs. 10.

$$EFF = 1 - \frac{C_{\text{target}}^{\text{GAM}} \times Imax}{C_{\text{target}}^{\text{GAM}} + IC50^{\text{GAM}}} \tag{10}$$

Where C_{target} is the target site concentration of MBi-5 , *IC50* the C_{target} that results in 50% inhibition of BACE1, *Imax* is the maximum response and *GAM* is the Hill coefficient. C_{target} was derived from the PK model as:

$$C_{\text{target}} = C_{\text{plasma}} \times \frac{AUC_{\text{CSF}}}{AUC_{\text{plasma}}} \tag{11}$$

Where AUC_{CSF} and AUC_{plasma} are the areas under the CSF and plasma concentration time curves, respectively. Here, C_{target} is assumed to follow the same profile as C_{plasma}, but at a level between C_{CSF} and C_{plasma}.

It is assumed that the system is in steady state when no treatment is given *(EFF=1)*. At the treatment free-state, the change of the variables with respect to time is:

$$\frac{d}{dt}APP = 0 \quad \frac{d}{dt}sAPP\alpha = 0 \quad \frac{d}{dt}sAPP\beta = 0 \quad \frac{d}{dt}A\beta_{40} = 0 \quad \frac{d}{dt}A\beta_{42} = 0 \tag{12}$$

These steady state conditions were used to derive part of the system parameters. From Eqs. 12 and Eqs. 5 it follows that the source of APP *(Rin_{APP})* is:

$$Rin_{APP} = (Rin\alpha + Rin\beta) \times APP_{base} \tag{13}$$

Where APP_{base} is the baseline level of APP, which is assumed to be equal to the sum of the

Downloaded from jpet.aspetjournals.org at ASPET Journals on April 10, 2024

JPET Fast Forward. Published on January 29, 2016 as DOI: 10.1124/jpet.115.230565
This article has not been copyedited and formatted. The final version may differ from this version.

baseline levels of sAPPα and sAPPβ, as it was assumed that there is no alternative proteolytic enzyme cleaving full length APP other than α-secretase and BACE1.

Using Eqs. 12 and Eqs. 6 the sAPPα formation rate (*Rin*α), equivalent to the α-secretase cleavage step, can be derived:

$$Rin\alpha = Rout_a \times \frac{sAPP\alpha_{base}}{APP_{base}} \tag{14}$$

Where sAPPα_{base} is the baseline level of sAPPα.

The sAPPβ formation rate (*Rin*β), equivalent to the BACE1 cleavage step, follows from Eqs. 12 and Eqs. 7:

$$Rin\beta = (Kin_{40} + Kin_{42}) \times \frac{sAPP\beta_{base}}{APP_{base}} \tag{15}$$

Where *sAPP*β_{base} is the baseline level of sAPPβ.

From Eqs. 12 and Eqs. 8 the Aβ40 formation rate (*Kin40*), equivalent to a γ-secretase cleavage step can be calculated:

$$Kin_{40} = Kout \times \frac{A\beta 40_{base}}{sAPP\beta_{base}} \tag{16}$$

Where *A*β*40*$_{\mathrm{base}}$ is the baseline level of Aβ40. sAPPβ_{base} is the baseline level of sAPPβ, used here as surrogate for the baseline level of C99.

From Eqs. 9 and Eqs. 12, with substitution of *Kout* from Eqs.16, the Aβ42 formation rate (*Kin42*), equivalent to a γ-secretase cleavage step, is deduced:

Downloaded from jpet.aspetjournals.org at ASPET Journals on April 10, 2024

JPET Fast Forward. Published on January 29, 2016 as DOI: 10.1124/jpet.115.230565
This article has not been copyedited and formatted. The final version may differ from this version.

$$Kin_{42} = Kin_{40} \times \frac{A\beta 42_{base}}{A\beta 40_{base}} \tag{17}$$

Where $A\beta 42_{\mathrm{base}}$ is the baseline level of Aβ42.

The model structure includes four transit compartments (Fig. 2), one for each biomarker measured in CSF (sAPPα, sAPPβ, Aβ40, Aβ42), to account for transport from the target site in the brain to CSF. These transit processes are described, in general, by Eqs. 18:

$$\frac{d}{dt} species_{CSF} = Kt \times (species - species_{CSF}) \tag{18}$$

Where *Kt* is the transit rate for the particular species (*KtAP* for sAPPα and sAPPβ and *KtAB* for Aβ40 and Aβ42).

The system defined above can now be extended to incorporate an Aβ_{O} pool for Aβ42 oligomerization. The addition of the Aβ_{O} pool to the model structure requires adaptation of Eqs. 9, describing Aβ42 dynamics. The exchange between the Aβ_{O} pool and the Aβ42 compartment is described by Eqs. 19 and Eqs. 20:

$$\frac{d}{dt} A\beta_{42} = Kin_{42} \times sAPP\beta - Kout_{42} \times A\beta_{42} - Kpl \times A\beta_{42} + Krev \times A\beta_{O} \tag{19}$$

$$\frac{d}{dt} A\beta_{O} = Kpl \times A\beta_{42} - Krev \times A\beta_{O} \tag{20}$$

Where *Kpl* and *Krev* are the Aβ42 oligomerization and dissociation rate, respectively, which are dependent on the baseline values of Aβ42 and the Aβ_{O} pool (A$\beta 42_{\mathrm{base}}$ and Aβ_{Obase}, resp.)

Downloaded from jpet.aspetjournals.org at ASPET Journals on April 10, 2024

JPET Fast Forward. Published on January 29, 2016 as DOI: 10.1124/jpet.115.230565
This article has not been copyedited and formatted. The final version may differ from this version.

according to Eqs. 21:

$$Krev = \frac{Kpl \times A\beta_{42base}}{A\beta_{Obase}} \tag{21}$$

Downloaded from jpet.aspetjournals.org at ASPET Journals on April 10, 2024

JPET Fast Forward. Published on January 29, 2016 as DOI: 10.1124/jpet.115.230565
This article has not been copyedited and formatted. The final version may differ from this version.

Results

Separate empiric models described response of each APP metabolite

Initially, empirical PK-PD models were developed to quantify the exposure-response relationships for each CSF APP metabolite (Aβ40, Aβ42, sAPPα and sAPPβ) of the BACEi MBi-5 in monkeys. The typical model structure of each APP metabolite-inhibitor combination consisted of a transit model with 1 or 2 compartments, with the drug effect modeled relative or subtractive to baseline using an Imax/Emax function. A summary overview of the results of these models is depicted in Table 1. The empirical models provided consistency of drug effects across APP metabolites (identified potencies Aβ40: 0.0254 μM (95% CI, 0.0246-0.0262); Aβ42: 0.0455 μM (95% CI, 0.0351-0.0559); sAPPβ: 0.0490 μM (95% CI, 0.0192-0.0788); sAPPα: 0.0265 μM (95% CI, 0.0135-0.0395)). The mean transit time through the compartments of the models was lower for Aβ40 and Aβ42 than for sAPPβ and sAPPα. This indicates that the response of Aβ40 and Aβ42 will appear earlier in CSF, even though sAPPβ is a sequentially earlier product of the amyloidogenic APP pathway.

A systems model to describe APP metabolite responses

A comprehensive compartmental PK-PD model, incorporating MBi-5 PK and CSF APP metabolites (Aβ40, Aβ42, sAPPα and sAPPβ) concentrations was developed to quantify APP metabolite responses to BACE1 inhibition in monkeys. The model is schematically presented in Fig. 2. The model described production, elimination, and brain-to-CSF transport of each APP metabolite, as well as their interrelationships. The rate of APP metabolism was assumed to be close to the maximal capacity of the enzymes involved (Nelson and Cox, 2000). Thus, APP production was approximated to follow zero-order kinetics. sAPPβ was used in the model structure as a surrogate substrate for C99 in the γ-secretase cleavage step. As both sAPPβ and C99 are products of the APP cleavage by BACE1, their formation rates should be the same and thus use of sAPPβ as a surrogate for C99 was justified. To account for transport from the target site in

Downloaded from jpet.aspetjournals.org at ASPET Journals on April 10, 2024

JPET Fast Forward. Published on January 29, 2016 as DOI: 10.1124/jpet.115.230565
This article has not been copyedited and formatted. The final version may differ from this version.

the brain to CSF, the model included one transit compartment for each APP metabolite. The drug effect was incorporated in the model as the inhibition of loss of the APP precursor pool, equivalent to the BACE1 cleavage step.

MBi-5 increased sAPPα and decreased sAPPβ and Aβ in a dose dependent manner

APP metabolite CSF concentrations showed a dose-dependent response in the presence of the BACEi. The dose-dependent increase of sAPPα and the corresponding decreases of sAPPβ and Aβ were described by the model with a single drug effect. A potency (IC_{50}) of 0.0256 μM (95% CI, 0.0137-0.0375) was identified. This value is close to the *in vitro* inhibition constant (*Ki*) of 10 nM for MBi-5 inhibition of purified BACE1 and also close to the IC_{50} for inhibition of Aβ production in intact cells of 24$\pm$6 nM (Dobrowolska et al., 2014a). When estimated, the maximal inhibition (Imax) was close to 1. Therefore Imax could be fixed to 1, indicating 100% inhibition of BACE1 at sufficient high drug concentrations. Figures 4 to 7 show the model description of each APP metabolite for each dose group.

Aβ_O pool required to account for differential effect on Aβ40 and Aβ42

A differential effect of BACE1 inhibition was observed for Aβ40 and Aβ42: a higher response is observed in the data for Aβ40 than for Aβ42 (e.g. Fig. 7E and 7G). This differential effect could be described by extending the model with an Aβ_O pool connected to the Aβ42 compartment, resulting in an adequate description of sAPPβ, sAPPα, Aβ40 and Aβ42 CSF concentration time profiles for each dose group (Fig. 4, 5, 6, 7, respectively). Incorporating the Aβ_O pool in the model improved the description of Aβ40 response for the 30 and 125 mg/kg dose group (compare Fig. 6E to Fig. 6F and Fig. 7E to Fig. 7F), as well as the description of the 125 mg/kg dose for Aβ42 response (compare Fig. 7G to Fig. 7H). Furthermore, the description of sAPPβ response for 125 mg/kg dose (compare Fig. 7C to Fig. 7D) was improved. Exchange of an Aβ40 monomer pool with an Aβ_O pool was evaluated, but could not be identified.

Downloaded from jpet.aspetjournals.org at ASPET Journals on April 10, 2024

JPET Fast Forward. Published on January 29, 2016 as DOI: 10.1124/jpet.115.230565
This article has not been copyedited and formatted. The final version may differ from this version.

Model parameters

The population parameters and intra- and interanimal variability were optimized for the study population and are depicted in Table 2. A sequence of models with interanimal variability on different parameters was tested and the results compared, in order to select the best random effects model structure. The final model included interanimal variability for the baseline of sAPPβ and the IC_{50} of MBi-5. Both were included as exponential in nature, reflecting lognormal distributions of the individual model parameters. As the baselines of the other APP metabolites were modeled as function of the baseline of sAPPβ, its interanimal variability reflects also on the other baselines. Residual variability was included for each APP metabolite (sAPPβ, sAPPα, Aβ40, Aβ42), as proportional error models, assuming that the residual errors are normally distributed. The identified residual variability was higher for Aβ40 and Aβ42 than for sAPPβ and sAPPα. System specific parameters could be distinguished from drug specific parameters (all correlations $<$0.95).

Incorporating the $A\beta_O$ pool in the model improved the description and did not affect the parameter estimate of the IC_{50} significantly: With $A\beta_O$ pool an IC_{50} of 0.0269 μM (95% CI, 0.0154-0.0384) was identified and without $A\beta_O$ pool the IC_{50} was 0.0256 μM (95% CI, 0.0137-0.0375). The incorporation of the $A\beta_O$ pool affected the Hill coefficient of the sigmoidal Imax concentration response relationship. The $A\beta_O$ pool resulted in a Hill coefficient slightly deviating from unity: With the $A\beta_O$ pool a Hill coefficient of 1.53 (95% CI, 1.14-1.92) was identified and without $A\beta_O$ pool the Hill coefficient was 1 (fixed). This mainly improved the description of the APP metabolite concentration response curves for the higher dose groups (Fig. 7).

Higher brain-to-CSF transport of Aβ

It was not possible to separate the rate of the γ-secretase cleavage from the brain-to-CSF trans-

Downloaded from jpet.aspetjournals.org at ASPET Journals on April 10, 2024

JPET Fast Forward. Published on January 29, 2016 as DOI: 10.1124/jpet.115.230565
This article has not been copyedited and formatted. The final version may differ from this version.

port. The transit rate for Aβ40 and Aβ42 was assumed to be equal and fast. Therefore, the transit rate from brain to CSF for Aβ40 and Aβ42 was fixed to an arbitrary high value (10 h^{-1}). Then, the Aβ half-life of 0.7 h reflects delays due to the γ-secretase cleavage step and brain-to-CSF transfer. For sAPPβ and sAPPα the transit rate was estimated to be 0.0985 h^{-1}. This value should be interpreted relative to the Aβ transit from brain-to-CSF. For sAPPα the brain-turnover (0.8 h) could be distinguished from the half-life of brain-to-CSF transfer (7.0 h). Aβ is transported from brain to CSF approximately 10^2-fold faster than sAPPα. As a result, the response of Aβ to drug treatment will appear earlier in CSF than the response of sAPPα, even though sAPPα is a sequentially earlier product of the APP pathway.

It was not possible to identify the brain-turnover of sAPPβ as a separate parameter. In the model structure, sAPPβ was used as a surrogate substrate for C99 in the γ-secretase cleavage step, driving the response of Aβ. Therefore, the γ-secretase cleavage step could not be separated from sAPPβ elimination.

APP metabolites interrelationships

The proteolytic cleavage rates of APP through the action of BACE1 (*Rin*β) and α-secretase (*Rin*α) were calculated from the model parameters according to Eqs. 15 and Eqs. 14 to be 0.314 h^{-1} and 0.404 h^{-1} indicating that 56% of full length APP is cleaved by α-secretase and 44% by BACE1. The formation rates of Aβ40 and Aβ42 were calculated according to Eqs. 16 and 17. The higher Kin_{40} (0.574 h^{-1}) than Kin_{42} (0.020 h^{-1}) is in line with previously reported findings of the ratio between Aβ42 and Aβ40 of about 1:10 in non-Alzheimer brain (Iwatsubo et al., 1994). A difference in Aβ40 and Aβ42 degradation rate (*Kout*) was also evaluated during the model development process, but this could not adequately capture the response profile of Aβ42.

The developed model could be used to predict biomarker interrelationships in response to BACE1 inhibition and visualize the response of APP and $A\beta_O$ (Fig. 3A) in brain. APP increases after BACE1 inhibition and appears to be shunted down the α-secretase pathway, resulting in an

Downloaded from jpet.aspetjournals.org at ASPET Journals on April 10, 2024

JPET Fast Forward. Published on January 29, 2016 as DOI: 10.1124/jpet.115.230565
This article has not been copyedited and formatted. The final version may differ from this version.

increase of sAPPα product. The elevation in sAPPα in the data drives the modeling conclusion that there is some increase in APP in the setting of BACE1 inhibition but it is fairly modest. The Aβ_{O} level decreases after BACE1 inhibition, indicating that there is reduced formation of Aβ_{O} by reduced levels of monomeric Aβ42 and that Aβ_{O} dissociates to monomeric Aβ42. The latter influences the shape of the Aβ42 response curve, which is different than the shape of the Aβ40 response curve.

For sAPPβ, sAPPβ, Aβ40 and Aβ42 the time courses of brain *versus* CSF responses were predicted (Fig. 3A and Fig. 3B, respectively), showing that the earlier appearance of Aβ response in CSF relative to sAPPα and sAPPβ arises from the slower brain to CSF transfer.

Downloaded from jpet.aspetjournals.org at ASPET Journals on April 10, 2024

JPET Fast Forward. Published on January 29, 2016 as DOI: 10.1124/jpet.115.230565
This article has not been copyedited and formatted. The final version may differ from this version.

Discussion

A systems model of the APP processing pathway was developed describing the interrelationships of Aβ40, Aβ42, sAPPα, and sAPPβ upon inhibition of BACE1 with MBi-5. All four APP metabolites provided consistent information regarding drug potency. The MBi-5 concentration-dependent decrease of the APP metabolites could be described by incorporating a single drug effect in the model: inhibition of the formation rate of sAPPβ, equivalent to the BACE1 cleavage step. The model supported the notion that MBi-5 can provide 100% inhibition of BACE1, consistent with a complete blockage of Aβ production at high drug concentrations. The fact that MBi-5 can provide 100% inhibition of BACE1, implies that there are no inherent mechanistic limitations of the APP pathway to blocking Aβ production. Therefore, reaching complete inhibition largely depends on drug properties such as having sufficient potency, bioavailability and tolerability.

The relatively large interanimal variability identified on the baseline level of sAPPβ (also reflecting on the baseline levels of the other APP metabolites) and the IC_{50} probably denotes the large intrinsic biological differences in APP processing between subjects. Residual variability was higher for Aβ40 and Aβ42 than for sAPPβ and sAPPα. Residual variability represents the uncertainty in the relationship between the concentrations predicted by the model and the observed concentration and includes any model misspecification error. The higher residual variability for Aβ could be related to the second cleavage step by γ-secretase, yielding Aβ. In the current analysis, no direct information was available regarding the γ-secretase cleavage step. This would require data from a γ-secretase inhibitor study. Such data may explain some of the residual variability identified for Aβ.

The systems model identified a higher brain-to-CSF transport of Aβ compared to sAPPα. This results is consistent with the identified lower mean transit time for Aβ40 and Aβ42 compared to sAPPα in the separate empirical models for each APP metabolite. The potencies identified in the empirical models were consistent with the single potency of 0.0256 μM (95%

Downloaded from jpet.aspetjournals.org at ASPET Journals on April 10, 2024

JPET Fast Forward. Published on January 29, 2016 as DOI: 10.1124/jpet.115.230565
This article has not been copyedited and formatted. The final version may differ from this version.

CI, 0.0137-0.0375) identified using the systems model.

In the systems model, the APP production was approximated to follow zero-order kinetics. In reality, APP production is regulated by various factors, above all the synaptic activity (Cheng et al., 2014). In the current analysis, no quantitative data on the factors involved in APP production was available. It was assumed that the APP production was close to the maximum. Consequently, subtle changes in APP regulation would have little impact on APP metabolites formation.

Our modeling results imply that 56% of full length APP is cleaved by α-secretase and 44% by BACE1. There is no quantitative data available from literature on the ratio of APP moving down the α-secretase pathway and BACE1 pathway. Dobrowlska et al. (2014) compared sAPPα and sAPPβ levels in human CSF from the lumbar region from cognitively normal and AD participants (Dobrowolska et al., 2014b). They identified a sAPPβ/sAPPα ratio of 0.59 $\pm$0.4 (n=15) in cognitively normal healthy controls. Wu et al. (2011) reported sAPPα and sAPPβ levels in human brain cortex samples from elderly subjects without AD (n=16) of 37.1 pmol/g and 50.8 pmol/g, respectively (Wu et al., 2011), resulting in a ratio of 0.73. However, both ratios do not directly reflect the ratio of APP cleaved by α-secretase and BACE1, as the steady state sAPPβ and sAPPα levels in brain are the result of multiple processes such as production, degradation and transfer from brain-to-CSF. Levels in CSF are also affected by transfer through the lumbar region. In the current analysis, the developed model facilitated the separation of the different processes involved.

The systems analysis points to a difference in biology of Aβ40 and Aβ42. Firstly, a lower formation rate for Aβ42 than for Aβ40 was identified. This is consistent with the composition of Aβ species reported for human CSF where the Aβ40 is the dominant isoform (Murphy et al., 1999). The relative production of Aβ40 and Aβ42 is probably regulated through changes in the γ-secretase cleavage site (Dolev et al., 2013; Murphy et al., 1999). Secondly, the model included an Aβ_O pool in brain for Aβ42 but not Aβ40. Inclusion of exchange of an Aβ42

Downloaded from jpet.aspetjournals.org at ASPET Journals on April 10, 2024

JPET Fast Forward. Published on January 29, 2016 as DOI: 10.1124/jpet.115.230565
This article has not been copyedited and formatted. The final version may differ from this version.

monomer pool with an Aβ_{O} pool could account for the differential effect of MBi-5 on Aβ40 and Aβ42 response observed in the data, in which the response for Aβ40 was higher than for Aβ42. Without incorporation of the Aβ_{O} pool in the model, the Aβ40 and Aβ42 response could not both be described adequately by a single drug effect. The identification of this Aβ_{O} constitutes the scientific basis for the identification of BACE1 inhibitor effects on higher ordered amyloid species. Due to the dissociation of Aβ42 oligomers to Aβ42 monomers during BACE1 inhibition the response for Aβ42 was lower than for Aβ40. The differential effect of the Aβ_{O} pool on Aβ42 is consistent with the biology of oligomer- and plaque formation where Aβ42 plays a more significant role than Aβ40 (Di Carlo et al., 2012). Aβ42 is the major constituent of plaque and other species such as oligomers (Iwatsubo et al., 1994; Jarrett et al., 1993).

The baseline level of the Aβ_{O} pool estimated by the model of 278 pM (1,255 pg/mL) should be interpreted as the level of Aβ42 monomers that is incorporated in the 'oligomer soup' in the brain, i.e. Aβ dimers, trimers and high molecular weight species (Benilova et al., 2012). Here, no distinction is made between oligomeric species, as the Aβ_{O} pool is modeled as a pool in equilibrium with monomeric Aβ42 without correction for the number of subunits in multimeric species comprising the Aβ_{O} pool.

The Aβ_{O} dissociation rate (*Krev*) of 1.308 $\times$ 10^{-5} s^{-1} identified here is relatively slow compared to the dissociation of Aβ aggregates acquired from *in vitro* analysis techniques. Gruning et al. (2013) detected the appearance of monomers from Aβ42 and Aβ40 protofibrils: the dissociation rate was 1.4×10^{-4} and $1.2\times$ $10-4$ s^{-1} for Aβ42 and Aβ40, respectively. Narayan et al. (2012) reported Aβ40 fibrils releasing soluble Aβ40 species at a rate of 9.3×10^{-5} s^{-1}. Sánchez et al. (2011) identified Aβ monomer off-rates of 0.6×10^{-2} and 1.0×10^{-2} s^{-1} for Aβ40 and Aβ42 fibrils. It is difficult to compare rates obtained *in vivo* to those determined using *in vitro* approaches, as the *in vitro* experimental settings can have major impact. Moreover, the comparability of the dissociation rates to the value obtained in the current analysis is limited, because no particular oligomeric species was characterized in the systems pharmacology

Downloaded from jpet.aspetjournals.org at ASPET Journals on April 10, 2024

JPET Fast Forward. Published on January 29, 2016 as DOI: 10.1124/jpet.115.230565
This article has not been copyedited and formatted. The final version may differ from this version.

approach.

Quantitative measurements of the response of $A\beta_O$ to drugs targeting the APP pathway, such as BACE1 inhibition, is of interest. Initial results of a new sensitive $A\beta$ oligomer assay (Savage et al., 2014) suggest an $A\beta_O$ baseline level of $\sim$1.5 pg/mL in rhesus CSF from the cisterna magna, which constitutes different oligomeric species (Mary Savage, Juliya Kalinina, unpublished observations). This number cannot be compared directly to the model derived $A\beta_O$ baseline of 1,255 pg/mL representing $A\beta$ subunits in the 'oligomer soup' in the brain. Also, the $A\beta$-oligomer assay may not pick up all oligomeric species or $A\beta_O$ may dissociate to monomers during sample preparation. Furthermore, it remains to be seen if CSF $A\beta_O$ measurements accurately reflect the brain $A\beta_O$ concentrations (Rosenblum, 2014). The hydrophobicity of oligomers may make them very low or absent in aqueous fluids as CSF (Yang et al., 2013). Recent data suggest that human CSF $A\beta_O$ range between 0.1 and 10 pg/mL and human brain $A\beta_O$ levels are 252 pg/mL in AD and 87 pg/mL in control brain (Savage et al., 2014). Other data suggest 1,000-fold higher concentrations of $A\beta_O$ than monomers in the soluble fraction of human AD cerebral cortex (Yang et al., 2013). Relative concentrations in CSF will not necessary reflect the relative concentrations in brain as oligomers are likely cleared to CSF much more slowly than monomeric $A\beta$. Additional dose-ranging studies of BACE1 inhibition in rhesus in which $A\beta_O$ response is quantified, are ongoing. It is anticipated that including such data in the systems pharmacology model analysis will elucidate the relationship between the $A\beta_O$ pool in the model and measurements of $A\beta_O$.

The identified $A\beta_O$ pool should be interpreted with caution as an $A\beta_O$ pool in rhesus may differ from an $A\beta_O$ pool in AD patients with plaque burden. Rhesus do not develop dementia and neurodegenerative changes that characterize AD (Heuer et al., 2012). It is almost certain that the rhesus used in this study had far less amyloid deposition than a human AD patient. Therefore, the most crucial question is the nature of the identified $A\beta_O$ pool in rhesus and its pathological relevance to AD in human. $A\beta$ oligomerization is a separate aggregation event.

Downloaded from jpet.aspetjournals.org at ASPET Journals on April 10, 2024

JPET Fast Forward. Published on January 29, 2016 as DOI: 10.1124/jpet.115.230565
This article has not been copyedited and formatted. The final version may differ from this version.

Certain oligomers are off-pathway species that do not further aggregate to amyloid fibrils. Coexistence of several oligomeric populations that do or do not propagate into fibrils is possible. If it can be demonstrated that there is a relationship between the soluble Aβ_{O} identified in rhesus and the AD brain-derived soluble Aβ_{O} and this could be correlated with neurotoxicity, then the relevance of Aβ_{O} in rhesus would be indisputable.

The lack of success of clinical trials targeting the APP pathway has been ascribed to the failure to reduce the level of toxic Aβ_{O} (Rosenblum, 2014). Plaques, toxic Aβ_{O} and Aβ peptides should be targeted to significantly reduce soluble Aβ load because of the relationship between these three. It has been hypothesized that by decreasing Aβ levels, soluble Aβ_{O} amounts are also reduced, in turn inducing the release of Aβ_{O} from plaques to restore the balance between Aβ_{O} in the plaques and the extracellular environment (Rosenblum, 2014).

The ability to identify and estimate the oligomerization effect through modeling suggested that these efforts to model the monomer pathway may also provide information on the higher ordered amyloid species. The ability to see this effect suggested that Aβ production inhibition by MBi-5 may also have the ability to draw down these forms as well as inhibit Aβ *de novo* production. In an APP transgenic mice study it has been demonstrated that BACE1 inhibition reduces amyloid plaque load (Kennedy and Hide, unpublished observations). This implies that if monomeric Aβ levels decrease as result of blocked Aβ production, Aβ_{O} dissociate to restore the equilibrium between monomeric Aβ and Aβ_{O}. To confirm this, incorporation of Aβ_{O} data into the model using rhesus data is ongoing.

A comprehensive model of the APP pathway describing the effects the BACEi MBi-5 has been established, taking into account the kinetics and interrelationships of sAPPα, sAPPβ, Aβ40 and Aβ42. The effect of BACE1 inhibition was incorporated in the model as inhibition of the formation rate of sAPPβ. As sAPPβ and C99 are both products of the same BACE1 cleavage step, the response of sAPPβ could be used as driver of Aβ response. However, sAPPβ and C99 could be subjected to different elimination processes as C99 remains membrane bound

Downloaded from jpet.aspetjournals.org at ASPET Journals on April 10, 2024

JPET Fast Forward. Published on January 29, 2016 as DOI: 10.1124/jpet.115.230565
This article has not been copyedited and formatted. The final version may differ from this version.

(Selkoe, 1999). The fact that the Hill coefficient of the concentration response relationship slightly deviates from unity may be a reflection of this simplification of the underlying biological system. To adequately separate the sequential cleavage steps of BACE1 and γ-secretase from other processes involved, data from a γ-secretase inhibitor study in CMP rhesus (Cook et al., 2010) will be added to inform the model further (ongoing).

As BACE1 is the initiating enzyme in Aβ production, its inhibition has been proposed to decrease the amount of cerebral Aβ and to subsequently prevent the development of Aβ-associated pathologies (Cole and Vassar, 2007). With the developed systems pharmacology model a deeper comprehension of the effects of BACEi on the APP processing pathway and the anticipated effect on Aβ_{O} was gained. Understanding these effects early in preclinical development could improve the anticipation of the magnitude of Aβ reducing effects in humans. The model forms the first step in developing a translational systems model to predict possible Aβ response of new drug candidates in human, based on their estimated potency in rhesus.

Downloaded from jpet.aspetjournals.org at ASPET Journals on April 10, 2024

JPET Fast Forward. Published on January 29, 2016 as DOI: 10.1124/jpet.115.230565
This article has not been copyedited and formatted. The final version may differ from this version.

Acknowledgments

The authors would like to thank Randall J. Bateman and Justyna A. Dobrowolska (Department of Neurology, Washington University, St. Louis, MO) for their input on the study design and data interpretation and Eric M. Parker (Merck Research Laboratories, Whitehouse Station, NJ) for critical comments on the manuscript.

Authorship Contributions

Participated in research design: Savage, Michener, Kennedy, Stone, Kleijn.

Conducted experiments: Michener.

Performed data analysis: Van Maanen, Van Steeg, Stone.

Wrote or contributed to the writing of the manuscript: Van Maanen, Van Steeg, Savage, Stone, Kennedy, Danhof.

Downloaded from jpet.aspetjournals.org at ASPET Journals on April 10, 2024

JPET Fast Forward. Published on January 29, 2016 as DOI: 10.1124/jpet.115.230565
This article has not been copyedited and formatted. The final version may differ from this version.

References

Beal, SL (2008) *NONMEM Users Guide: Introduction to Version VI*, GloboMax ICON Development Solutions, Ellicott City, MD.

Benilova, I, Karran, E, and De Strooper, B (2012) The toxic Aβ oligomer and Alzheimer's disease: an emperor in need of clothes. *Nat Neurosci* **15**(3):349–357.

Cheng, X, Wu, J, Geng, M, and Xiong, J (2014) The role of synaptic activity in the regulation of amyloid beta levels in Alzheimer's disease. *Neurobiol Aging* **35**(6):1217–1232.

Cole, SL and Vassar, R (2007) The basic biology of BACE1: A key therapeutic target for Alzheimer's disease. *Curr Genomics* **8**(8):509–530.

Cook, JJ, Wildsmith, KR, Gilberto, DB, Holahan, MA, Kinney, GG, Mathers, PD, Michener, MS, Price, EA, Shearman, MS, Simon, AJ, Wang, JX, Wu, G, Yarasheski, KE, and Bateman, RJ (2010) Acute γ-secretase inhibition of nonhuman primate CNS shifts amyloid precursor protein (APP) metabolism from amyloid-β production to alternative APP fragments without amyloid-β rebound. *J Neurosci* **30**(19):6743–50.

Danhof, M, Alvan, G, Dahl, SG, Kuhlmann, J, and Paintaud, G (2005) Mechanism-based pharmacokinetic-pharmacodynamic modeling - A new classification of biomarkers. *Pharm Res* **22**(9):1432–7.

Danhof, M, De Jongh, J, De Lange, EC, Della Pasqua, O, Ploeger, BA, and Voskuyl, RA (2007) Mechanism-based pharmacokinetic-pharmacodynamic modeling: biophase distribution, receptor theory, and dynamical systems analysis. *Annu Rev Pharmacol Toxicol* **47**:357–400.

Di Carlo, M, Giacomazza, D, and San Biagio, PL (2012) Alzheimer's disease: biological aspects, therapeutic perspectives and diagnostic tools. *J Phys Condens Matter* **24**(24):244102.

Downloaded from jpet.aspetjournals.org at ASPET Journals on April 10, 2024

JPET Fast Forward. Published on January 29, 2016 as DOI: 10.1124/jpet.115.230565
This article has not been copyedited and formatted. The final version may differ from this version.

Dobrowolska, JA, Michener, MS, Wu, G, Patterson, BW, Chott, R, Ovod, V, Pyatkivskyy, Y, Wildsmith, KR, Kasten, T, Mathers, P, Dancho, M, Lennox, C, Smith, BE, Gilberto, D, McLoughlin, D, Holder, DJ, Stamford, AW, Yarasheski, KE, Kennedy, ME, Savage, MJ, and Bateman, RJ (2014) CNS amyloid-β, soluble APP-α and -β kinetics during BACE inhibition. *J Neurosci* **34**(24):8336–8346.

Dobrowolska, JA, Kasten, T, Huang, Y, Benzinger, TL, Sigurdson, W, Ovod, V, Morris, JC, and Bateman, RJ (2014) Diurnal patterns of soluble amyloid precursor protein metabolites in the human central nervous system. *PLoS One* **9**(3):e89998.

Dolev, I, Fogel, H, Milshtein, H, Berdichevsky, Y, Lipstein, N, Brose, N, Gazit, N, and Slutsky, I (2013) Spike bursts increase amyloid-β 40/42 ratio by inducing a presenilin-1 conformational change. *Nat Neurosci* **16**(5):587–95.

Esler, WP and Wolfe, MS (2001) A portrait of Alzheimer secretases - New features and familiar faces. *Science* **293**(5534):1449–54.

Esparza, TJ, Zhao, H, Cirrito, JR, Cairns, NJ, Bateman, RJ, Holtzman, DM, and Brody, DL (2013) Amyloid-beta oligomerization in Alzheimer dementia vs. high pathology controls. *Ann Neurol* **73**(1):104–119.

Gilberto, DB, Zeoli, AH, Szczerba, PJ, Gehret, JR, Holahan, MA, Sitko, GR, Johnson, CA, Cook, JJ, and Motzel, SL (2003) An alternative method of chronic cerebrospinal fluid collection via the cisterna magna in conscious rhesus monkeys. *Contemp Top Lab Anim Sci* **42**(4):53–59.

Grüning, CSR, Klinker, S, Wolff, M, Schneider, M, Toksöz, K, Klein, AN, Nagel-Steger, L, Willbold, D, and Hoyer, W (2013) The off-rate of monomers dissociating from amyloid-β protofibrils. *J Biol Chem* **288**(52):37104–11.

Hardy, J and Selkoe, DJ (2002) The amyloid hypothesis of Alzheimer's disease: progress and problems on the road to therapeutics. *Science* **297**(5580):353–6.

Downloaded from jpet.aspetjournals.org at ASPET Journals on April 10, 2024

JPET Fast Forward. Published on January 29, 2016 as DOI: 10.1124/jpet.115.230565
This article has not been copyedited and formatted. The final version may differ from this version.

Heuer, E, Rosen, RF, Cintron, A, and Walker, LC (2012) Nonhuman primate models of Alzheimer-like cerebral proteopathy. *Curr Pharm Des* **18**(8):1159–1169.

Husain, MM, Kenneth, T, Siddique, H, and McClintock, SM (2008) Present and prospective clinical therapeutic regimens for Alzheimer's disease. *Neuropsychiatr Dis Treat* **4**(4):765–777.

Iwatsubo, T, Odaka, A, Suzuki, N, Mizusawa, H, Nukina, N, and Ihara, Y (1994) Visualization of Aβ42(43) and Aβ40 in senile plaques with end-specific Aβ monoclonals: evidence that an initially deposited species is Aβ42(43). *Neuron* **13**(1):45–53.

Jack, CR and Holtzman, DM (2013) Biomarker modeling of Alzheimer's disease. *Neuron* **80** (6):1347–1358.

Janson, J, Eketjäll, S, Tunblad, K, Jeppsson, F, Von Berg, S, Niva, C, Radesäter, AC, Fälting, J, and Visser, SA (2014) Population PKPD modeling of BACE1 inhibitor-induced reduction in Aβ levels *in vivo* and correlation to in vitro potency in primary cortical neurons from mouse and guinea pig. *Pharm Res* **31**(3):670–83.

Jarrett, JT, Berger, EP, and Lansbury, PT (1993) The carboxy terminus of the β amyloid protein is critical for the seeding of amyloid formation: Implications for the pathogenesis of Alzheimer's disease. *Biochemistry* **32**(18):4693–4697.

Klein, WL (2013) Synaptotoxic amyloid-β oligomers: a molecular basis for the cause, diagnosis, and treatment of Alzheimer's disease? *J Alzheimers Dis* **33**:S49–S65.

Liu, X, Wong, H, Scearce-Levie, K, Watts, RJ, Coraggio, M, Shin, YG, Peng, K, Wildsmith, KR, Atwal, JK, Mango, J, Schauer, SP, Regal, K, Hunt, KW, Thomas, AA, Siu, M, Lyssikatos, J, Deshmukh, G, and Hop, CE (2013) Mechanistic pharmacokinetic-pharmacodynamic modeling of BACE1 inhibition in monkeys: development of a predictive model for amyloid precursor protein processing. *Drug Metab Dispos* **41**(7):1319–28.

Downloaded from jpet.aspetjournals.org at ASPET Journals on April 10, 2024

JPET Fast Forward. Published on January 29, 2016 as DOI: 10.1124/jpet.115.230565
This article has not been copyedited and formatted. The final version may differ from this version.

Lu, Y, Riddell, D, Hajos-Korcsok, E, Bales, K, Wood, KM, Nolan, CE, Robshaw, AE, Zhang, L, Leung, L, Becker, SL, Tseng, E, Barricklow, J, Miller, EH, Osgood, S, O'Neill, BT, Brodney, MA, Johnson, DS, and Pettersson, M (2012) Cerebrospinal fluid amyloid-β (Aβ) as an effect biomarker for brain Aβ lowering verified by quantitative preclinical analyses. *J Pharmacol Exp Ther* **342**(2):366–75.

Lu, Y, Barton, HA, Leung, L, Zhang, L, Hajos-Korcsok, E, Nolan, CE, Liu, J, Becker, SL, Wood, KM, Robshaw, AE, Taylor, CK, O'Neill, BT, Brodney, MA, and Riddell, D (2013) Cerebrospinal fluid β-amyloid turnover in the mouse, dog, monkey and human evaluated by systematic quantitative analyses. *Neurodegener Dis* **12**(1):36–50.

Mc Donald, JM, Savva, GM, Brayne, C, Welzel, AT, Forster, G, Shankar, GM, Selkoe, DJ, Ince, PG, and Walsh, DM (2010) The presence of sodium dodecyl sulphate-stable Aβ dimers is strongly associated with Alzheimer-type dementia. *Brain* **133**:1328–41.

Murphy, MP, Hickman, LJ, Eckman, CB, Uljon, SN, Wang, R, and Golde, ET (1999) γ-Secretase, evidence for multiple proteolytic activities and influence of membrane positioning of substrate on generation of amyloid β peptides of varying length. *J Biol Chem* **274**(17): 11914–11923.

Narayan, P, Orte, A, Clarke, RW, Bolognesi, B, Hook, S, Ganzinger, KA, Meehan, S, Wilson, MR, Dobson, CM, and Klenerman, D (2012) The extracellular chaperone clusterin sequesters oligomeric forms of the amyloid-β1-40 peptide. *Nat Struct Mol Biol* **19**(1):79–83.

Nelson, DL and Cox, MM (2000) *Lehninger Principles of Biochemistry*, 3rd ed. Worth Publishers, New York.

Parkinson, J, Ploeger, B, Appelkvist, P, Bogstedt, A, Dillner Bergstedt, K, Eketjäll, S, and Visser, SA (2013) Modeling of age-dependent amyloid accumulation and γ-secretase inhibition

Downloaded from jpet.aspetjournals.org at ASPET Journals on April 10, 2024

JPET Fast Forward. Published on January 29, 2016 as DOI: 10.1124/jpet.115.230565
This article has not been copyedited and formatted. The final version may differ from this version.

of soluble and insoluble Aβ in a transgenic mouse model of amyloid deposition. *Pharmacol Res Perspect* **1**(2):e00012.

Podlisny, MB, Tolan, DR, and Selkoe, DJ (1991) Homology of the amyloid beta protein precursor in monkey and human supports a primate model for beta amyloidosis in Alzheimer's disease. *Am J Pathol* **138**(6):1423–1435.

Portelius, E, Mattsson, N, Andreasson, U, Blennow, K, and Zetterberg, H (2011) Novel Aβ isoforms in Alzheimer's disease - Their role in diagnosis and treatment. *Curr Pharm Des* **17** (25):2594–2602.

Potter, R, Patterson, BW, Elbert, DL, Ovod, V, Kasten, T, Sigurdson, W, Mawuenyega, K, Blazey, T, Goate, A, Chott, R, Yarasheski, KE, Holtzman, DM, Morris, JC, Benzinger, TL, and Bateman, RJ (2013) Increased *in vivo* Amyloid-β42 production, exchange, and irreversible loss in Presenilin Mutations Carriers. *Sci Transl Med* **5**(189):189ra77.

Rosenblum, WI (2014) Why Alzheimer trials fail: removing soluble oligomeric beta amyloid is essential, inconsistent, and difficult. *Neurobiol Aging* **35**(5):969–974.

Sánchez, L, Madurga, S, Pukala, T, Vilaseca, M, López-Iglesias, C, Robinson, CV, Giralt, E, and Carulla, N (2011) Aβ40 and Aβ42 amyloid fibrils exhibit distinct molecular recycling properties. *J Am Chem Soc* **133**(17):6505–6508.

Sankaranarayanan, S, Holahan, MA, Colussi, D, Crouthamel, MC, Devanarayan, V, Ellis, J, Espeseth, A, Gates, AT, Graham, SL, Gregro, AR, Hazuda, D, Hochman, JH, Holloway, K, Jin, L, Kahana, J, Lai, MT, Lineberger, J, McGaughey, G, Moore, KP, Nantermet, P, Pietrak, B, Price, EA, Rajapakse, H, Stauffer, S, Steinbeiser, MA, Seabrook, G, Selnick, HG, Shi, XP, Stanton, MG, Swestock, J, Tugusheva, K, Tyler, KX, Vacca, JP, Wong, J, Wu, G, Xu, M, Cook, JJ, and Simon, AJ (2009) First demonstration of cerebrospinal fluid and plasma Aβ lowering

Downloaded from jpet.aspetjournals.org at ASPET Journals on April 10, 2024

JPET Fast Forward. Published on January 29, 2016 as DOI: 10.1124/jpet.115.230565
This article has not been copyedited and formatted. The final version may differ from this version.

with oral administration of a β-site amyloid precursor protein-cleaving enzyme 1 inhibitor in nonhuman primates. *J Pharmacol Exp Ther* **328**(1):131–140.

Savage, MJ, Kalinina, J, Wolfe, A, Tugusheva, K, Korn, R, Cash-Mason, T, Maxwell, JW, Hatcher, NG, Haugabook, SJ, Wu, G, Howell, BJ, Renger, JJ, Shughrue, PJ, and McCampbell, A (2014) A sensitive Aβ oligomer assay discriminates Alzheimer's and aged control cerebrospinal fluid. *J Neurosci* **34**(8):2884–97.

Selkoe, DJ (1999) Translating cell biology into therapeutic advances in Alzheimer's disease. *Nature* **399**(6738 Suppl):A23–31.

Wiltfang, J, Esselmann, H, Bibl, M, Smirnov, A, Otto, M, Paul, S, Schmidt, B, Klafki, HW, Maler, M, Dyrks, T, Bienert, M, Beyermann, M, Ruther, E, and Kornhuber, J (2002) Higly conserved and disease-specific patterns of carboxyterminally truncated Aβ peptides 1-37/38/39 in addition to 1-40/42 in Alzheimer's disease and in patients with chronic neuroinflammation. *J Neurochem* **81**(3):481–496.

Wu, G, Sankaranarayanan, S, Hsieh, SHK, Simon, AJ, and Savage, MJ (2011) Decrease in brain soluble amyloid precursor protein β (sAPPβ) in Alzheimer's disease cortex. *J Neurosci Res* **89**(6):822–32.

Yan, R and Vassar, R (2014) Targeting the β secretase BACE1 for Alzheimer's disease therapy. *Lancet Neurol* **13**(3):319–329.

Yang, T, Hong, S, O'Malley, T, Sperling, RA, Walsh, DM, and Selkoe, DJ (2013) New ELISAs with high specificity for soluble oligomers of amyloid β-protein detect natural Aβ oligomers in human brain but not CSF. *Alzheimers Dement* **9**(2):99–112.

Downloaded from jpet.aspetjournals.org at ASPET Journals on April 10, 2024

JPET Fast Forward. Published on January 29, 2016 as DOI: 10.1124/jpet.115.230565
This article has not been copyedited and formatted. The final version may differ from this version.

Figure Legends

Figure 1. Schematic representation of the amyloid hypothesis of AD. In the APP processing pathway, full length APP is cleaved by BACE1 (β-sec) or α-secretase (α-sec) to form sAPPβ and C99 or sAPPα and C83. C99 is then cleaved by γ-secretase (γ-sec) to form Aβ. The amyloid hypothesis states that an imbalance in production and clearance of Aβ can result in aggregation of Aβ42 fragments into amyloid plaque.

blue circles: APP metabolites measured in CSF.

Figure 2. Schematic of systems model of APP processing. The model comprised nine compartments: Five biomarker compartments in brain *(yellow circles)* and four transit compartments from brain to CSF *(white circles)*. Four biomarkers were measured in CSF (sAPPα, sAPPβ, Aβ40 and Aβ42), indicated by the blue boxes. The extended model included additionally an Aβ_{O} compartment *(dashed circle)*. The drug effect *(EFF)* inhibited *Rin*β. As driver of biomarker response C_{target} was used, which was derived from the PK model (see Supplemental Material). sAPPβ was used in the model structure as a surrogate substrate of C99 in the γ-secretase cleavage step.

APP: Aβ-precursor protein; *A*β: amyloid-β-peptide; C_{target}: drug concentration target site; Kin_{40}: Aβ40 formation rate; Kin_{42}: Aβ42 formation rate; *Kout*: Aβ degradation rate; *Kpl*: Oligomerization rate; *Krev*: Aβ_{O} dissociation rate; *KtAB*: transit rate Aβ from brain to CSF; *KtAP*: transit rate sAPPα and sAPPβ from brain to CSF; *RinAPP*: zero order input constant for APP; *Rin*α: sAPPα formation rate; *Rin*β: sAPPβ formation rate; *Rout*: sAPPβ degradation rate; *Routa*: sAPPα degradation rate.

Figure 3. Graphical insight into the biomarker responses in brain and CSF, using the identified systems model of the APP processing pathway. The biomarker responses in brain and CSF are predicted after a single dose of 125 mg MBi-5, using the typical parameter estimates.

APP grey dotdashed line; *sAPP*α red solid line; *sAPP*β black solid line; *A*β*40* green solid line; Aβ_{O} grey dotted line; *A*β*42* blue solid line.

Downloaded from jpet.aspetjournals.org at ASPET Journals on April 10, 2024

JPET Fast Forward. Published on January 29, 2016 as DOI: 10.1124/jpet.115.230565
This article has not been copyedited and formatted. The final version may differ from this version.

Figure 4. Placebo. Visual predictive check of biomarker response *vs.* time profile of placebo in the rhesus with 90% confidence interval. Predictions were performed with model without $A\beta_O$ compartment ((A), (B), (C), (D)). Predictions performed with model with $A\beta_O$ pool had identical results (not shown). Observation sample size: n=114 for each APP metabolite from 6 monkeys collected over 7 days.

Plus-symbols represent observed measurements. Dotted line corresponds to the median observed profile. Solid lines show the median simulated profiles. The longs-dashed lines correspond to the 90% prediction intervals obtained from 1000 individual simulated profiles.

Figure 5. Dose 10 mg/kg. Visual predictive check of biomarker response *vs.* time profile of MBi-5 in the rhesus with 90% confidence interval. Predictions were performed with model with ((B), (D), (F), (H)) and without ((A), (C), (E), (G)) $A\beta_O$ compartment. Observation sample size: n=114 for each APP metabolite from 6 monkeys collected over 7 days.

Plus-symbols represent observed measurements. Dotted line corresponds to the median observed profile. Solid lines show the median simulated profiles. The longs-dashed lines correspond to the 90% prediction intervals obtained from 1000 individual simulated profiles.

Figure 6. Dose 30 mg/kg. Visual predictive check of biomarker response *vs.* time profile of MBi-5 in the rhesus with 90% confidence interval. Predictions were performed with model with ((B), (D), (F), (H)) and without ((A), (C), (E), (G)) $A\beta_O$ compartment.Observation sample size: n=114 for each APP metabolite from 6 monkeys collected over 7 days.

Plus-symbols represent observed measurements. Dotted line corresponds to the median observed profile. Solid lines show the median simulated profiles. The longs-dashed lines correspond to the 90% prediction intervals obtained from 1000 individual simulated profiles.

Figure 7. Dose 125 mg/kg. Visual predictive check of biomarker response *vs.* time profile of MBi-5 in the rhesus with 90% confidence interval. Predictions were performed with model with ((B), (D), (F), (H)) and without ((A), (C), (E), (G)) $A\beta_O$ compartment. Observation sample

Downloaded from jpet.aspetjournals.org at ASPET Journals on April 10, 2024

JPET Fast Forward. Published on January 29, 2016 as DOI: 10.1124/jpet.115.230565
This article has not been copyedited and formatted. The final version may differ from this version.

size: n=114 for each APP metabolite from 6 monkeys collected over 7 days.

Plus-symbols represent observed measurements. Dotted line corresponds to the median observed profile. Solid lines show the median simulated profiles. The longs-dashed lines correspond to the 90% prediction intervals obtained from 1000 individual simulated profiles.

Downloaded from jpet.aspetjournals.org at ASPET Journals on April 10, 2024

JPET Fast Forward. Published on January 29, 2016 as DOI: 10.1124/jpet.115.230565
This article has not been copyedited and formatted. The final version may differ from this version.

Tables

Downloaded from jpet.aspetjournals.org at ASPET Journals on April 10, 2024

JPET Fast Forward. Published on January 29, 2016 as DOI: 10.1124/jpet.115.230565
This article has not been copyedited and formatted. The final version may differ from this version.

Table 1: Summary parameters of the separate empiric model fits for each APP metabolite

PARAMETER	DESCRIPTION	UNIT	APP METABOLITE			
			Aβ40	Aβ42	sAPPα	sAPPβ
baseline	baseline	pM	722	24.8	1040	1190
IM/EM	maximal inhibition / effect		100%[a]	20.4 pM	167%	100%[a]
IC_{50}/EC_{50}	median inhibition / effect concentration	μM	0.0254	0.0455	0.0265	0.0490
			(*CV 1.63%*)	(*CV 11.6%*)	(*CV 25.0%*)	(*CV 31.0%*)
GAM	Hill coefficient		1[a]	1[a]	1[a]	1[a]
MTT[b]	Mean transit time	h	5.155	3.597	15.873	19.417

[a] Fixed.

[b] $MTT = \frac{1}{Kt} \times (n+1)$, where *n* is the number of transit compartments and *Kt* is the transit rate.

Downloaded from jpet.aspetjournals.org at ASPET Journals on April 10, 2024

JPET Fast Forward. Published on January 29, 2016 as DOI: 10.1124/jpet.115.230565
This article has not been copyedited and formatted. The final version may differ from this version.

Table 2: Population parameter estimates including coefficient of variation (CV%) for the extended model with Aβ_{O} pool

PARAMETER	DESCRIPTION	VALUE	UNIT	CV%
Structural parameters				
sAPPβ_{base}	baseline sAPPβ	1.19×10^3	pM	11.6
Fbase$_{\mathrm{A}\beta 40}$[b]	Aβ40 baseline as fraction of sAPPβ_{base}	0.611		12.3
Fbase$_{\mathrm{A}\beta 42}$[c]	Aβ42 baseline as fraction of sAPPβ_{base}	0.0210		8.38
Fbase$_{\mathrm{sAPP}\alpha}$[d]	sAPPα baseline as fraction of sAPPβ_{base}	0.894		2.84
Kout	degradation rate Aβ40 and Aβ42	0.940	h^{-1}	13.6
Rout$_{\mathrm{a}}$	degradation rate sAPPα	0.856	h^{-1}	30.8
KtAP	transit rate sAPPα and sAPPβ	0.0985	h^{-1}	2.82
KtAB[a]	transit rate Aβ	10	h^{-1}	
IM[a]	maximal inhibition (Imax)	1		
IC_{50}	median inhibition concentration	0.0269	μM	21.8
GAM	Hill coefficient	1.53		13.1
Kpl	oligomerization rate	0.524	h^{-1}	20.0
A$\beta_{\mathrm{O\,base}}$	baseline Aβ_{O}	278	pM	41.0
Interanimal variability				
$\omega^2_{\mathrm{BSAPb}}$[e]	Interanimal variability sAPPβ baseline	0.0568		30.1
$\omega^2_{\mathrm{IC_{50}}}$[e]	Interanimal variability IC50	0.279		35.5
Residual error				
$\sigma^2_{\mathrm{A}\beta 40}$[f]	Residual variability Aβ40	0.240		12.7
$\sigma^2_{\mathrm{A}\beta 42}$[f]	Residual variability Aβ42	0.161		12.4
$\sigma^2_{\mathrm{sAPP}\beta}$[f]	Residual variabilty sAPPβ	0.0621		23.5
$\sigma^2_{\mathrm{sAPP}\alpha}$[f]	Residual variability sAPPα	0.0634		10.6

[a] Fixed.

[b] A$\beta 40_{\mathrm{base}}$=Fbase$_{\mathrm{A}\beta 40}\times$ sAPPβ_{base}.

[c] A$\beta 42_{\mathrm{base}}$=Fbase$_{\mathrm{A}\beta 42}$ $\times$ sAPPβ_{base}.

[d] sAPPα_{base}=Fbase$_{\mathrm{sAPP}\alpha}$ $\times$ sAPPβ_{base}.

[e] Interanimal variability is assumed to follow a normal distribution with mean zero and variance ω^2.

[f] Residual variability is assumed to follow a normal distribution with mean zero and variance σ^2.

Downloaded from jpet.aspetjournals.org at ASPET Journals on April 10, 2024

JPET Fast Forward. Published on January 29, 2016 as DOI: 10.1124/jpet.115.230565
This article has not been copyedited and formatted. The final version may differ from this version.

Figures

Figure 1

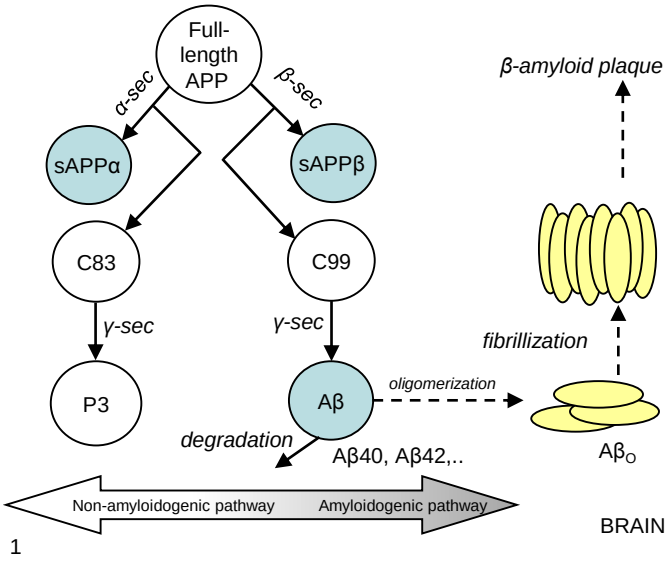

1

Downloaded from jpet.aspetjournals.org at ASPET Journals on April 10, 2024

JPET Fast Forward. Published on January 29, 2016 as DOI: 10.1124/jpet.115.230565
This article has not been copyedited and formatted. The final version may differ from this version.

Figure 2

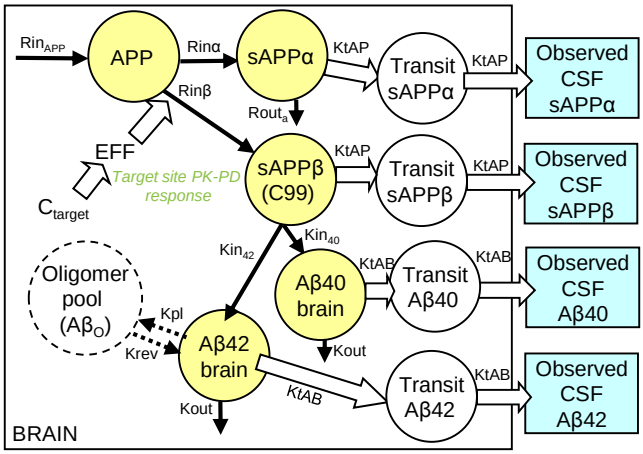

2

Downloaded from jpet.aspetjournals.org at ASPET Journals on April 10, 2024

JPET Fast Forward. Published on January 29, 2016 as DOI: 10.1124/jpet.115.230565
This article has not been copyedited and formatted. The final version may differ from this version.

Figure 3

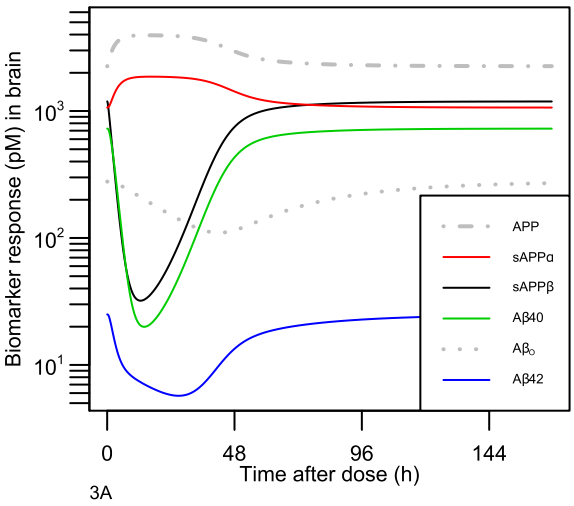

(A) brain

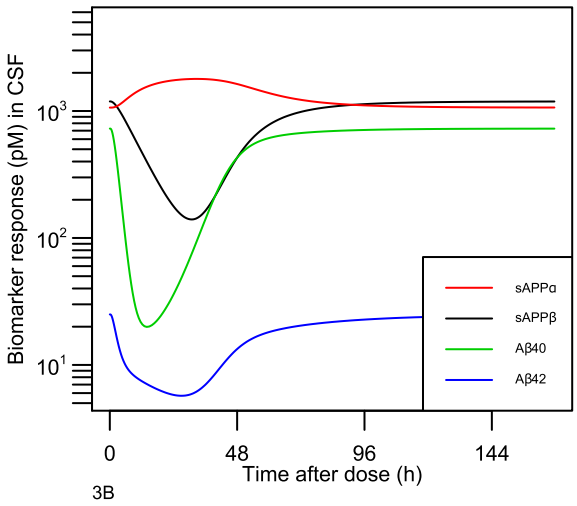

(B) CSF

Downloaded from jpet.aspetjournals.org at ASPET Journals on April 10, 2024

JPET Fast Forward. Published on January 29, 2016 as DOI: 10.1124/jpet.115.230565
This article has not been copyedited and formatted. The final version may differ from this version.

Figure 4

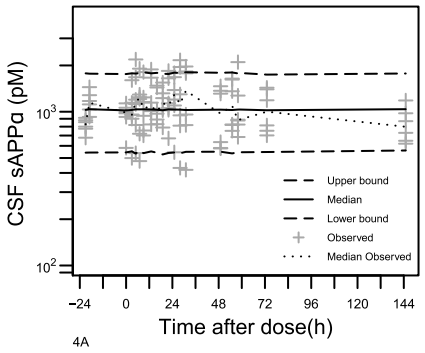

(A) sAPPα

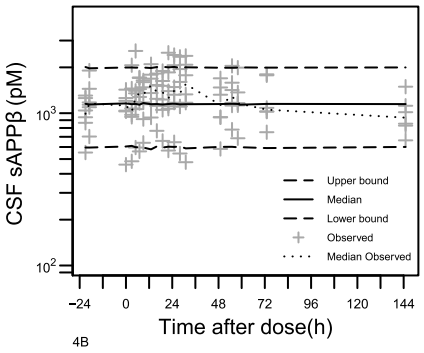

(B) sAPPβ

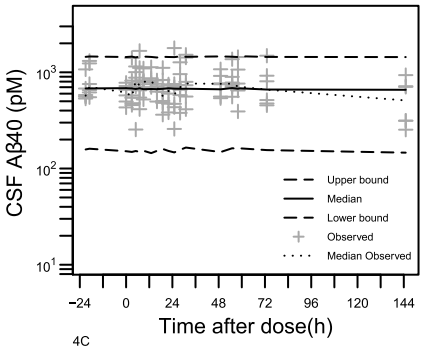

(C) Aβ40

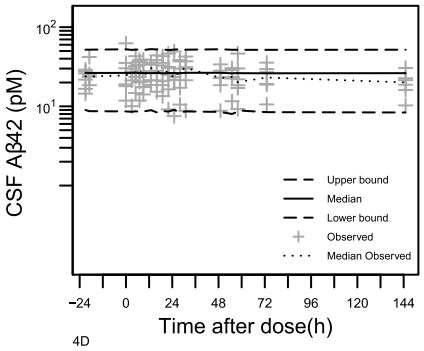

(D) Aβ42

Downloaded from jpet.aspetjournals.org at ASPET Journals on April 10, 2024

JPET Fast Forward. Published on January 29, 2016 as DOI: 10.1124/jpet.115.230565
This article has not been copyedited and formatted. The final version may differ from this version.

Figure 5

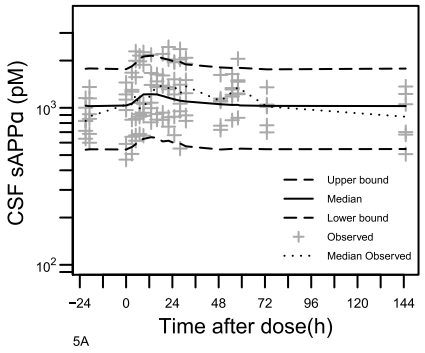

(A) sAPPα

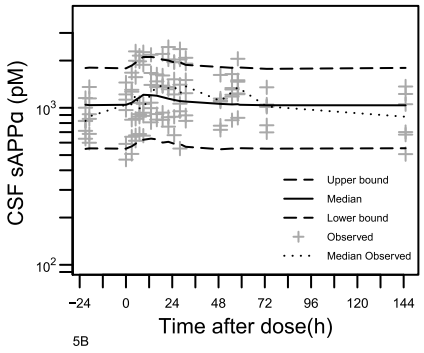

(B) sAPPα (With Aβ_{O})

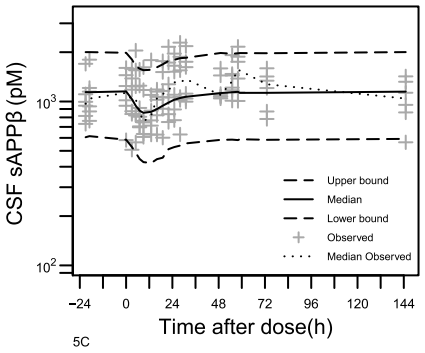

(C) sAPPβ

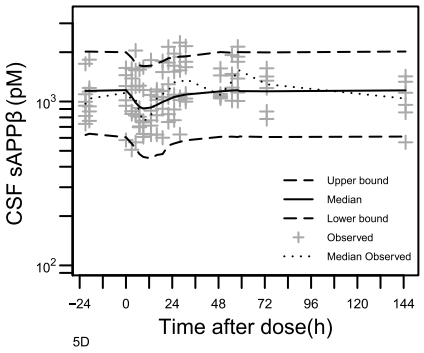

(D) sAPPβ (With Aβ_{O})

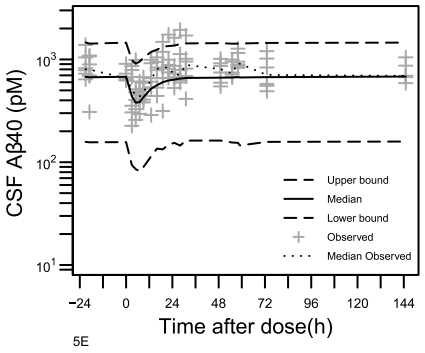

(E) Aβ40

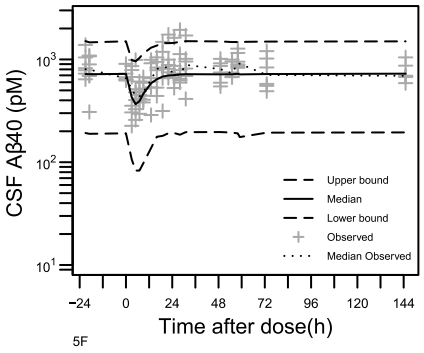

(F) Aβ40 (With Aβ_{O})

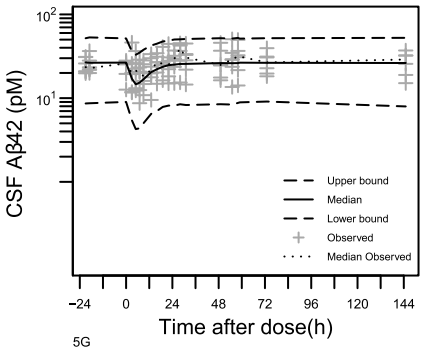

(G) Aβ42

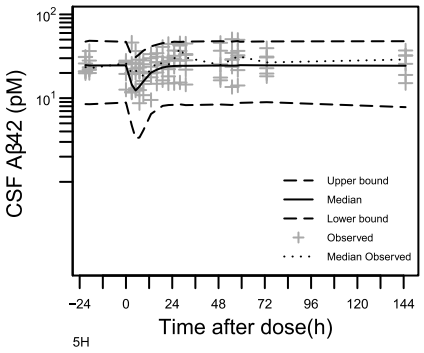

(H) Aβ42 (With Aβ_{O})

Downloaded from jpet.aspetjournals.org at ASPET Journals on April 10, 2024

JPET Fast Forward. Published on January 29, 2016 as DOI: 10.1124/jpet.115.230565
This article has not been copyedited and formatted. The final version may differ from this version.

Figure 6

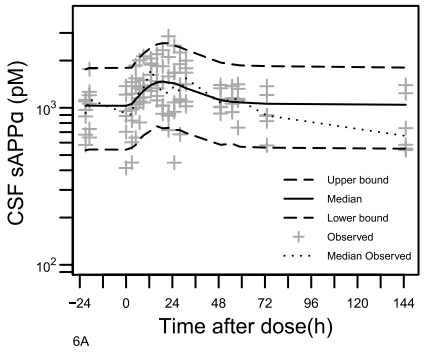

(A) sAPPα

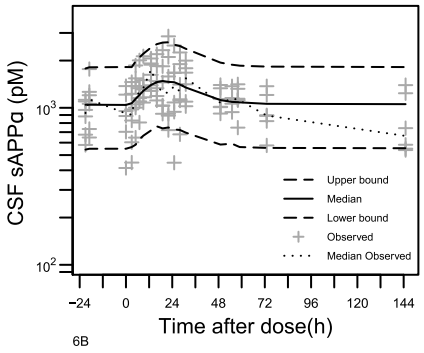

(B) sAPPα (With Aβ_{O})

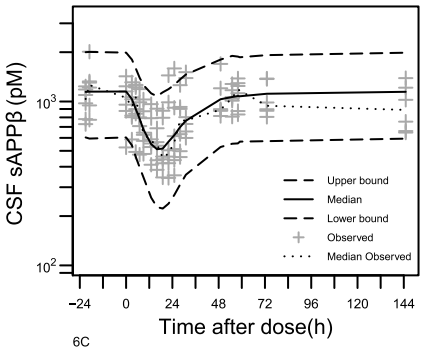

(C) sAPPβ

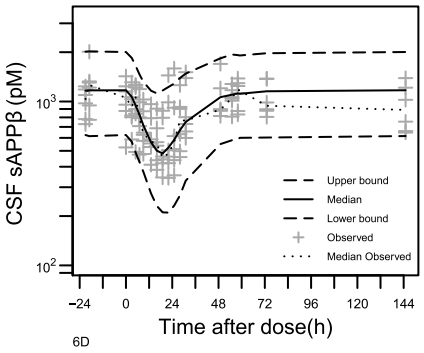

(D) sAPPβ (With Aβ_{O})

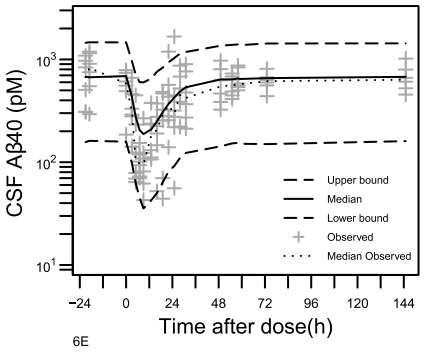

(E) Aβ40

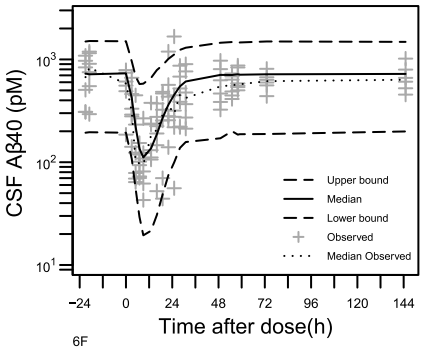

(F) Aβ40 (With Aβ_{O})

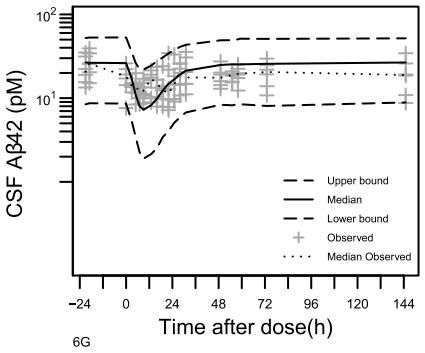

(G) Aβ42

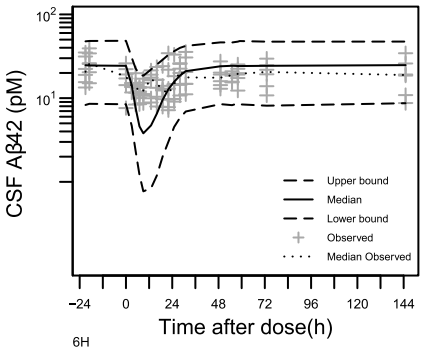

(H) Aβ42 (With Aβ_{O})

Downloaded from jpet.aspetjournals.org at ASPET Journals on April 10, 2024

JPET Fast Forward. Published on January 29, 2016 as DOI: 10.1124/jpet.115.230565
This article has not been copyedited and formatted. The final version may differ from this version.

Figure 7

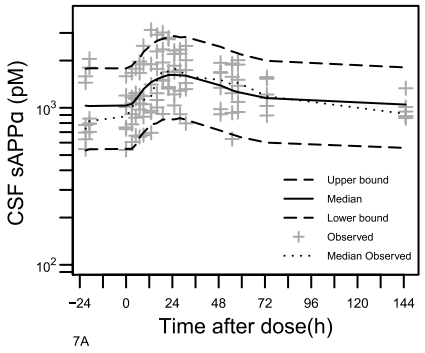

(A) sAPPα

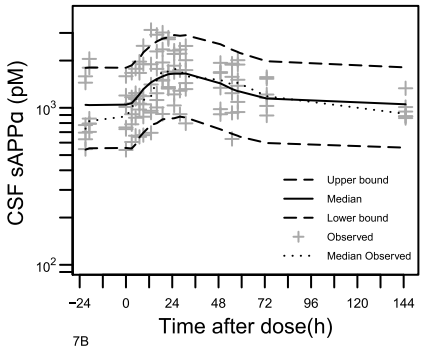

(B) sAPPα (With Aβ_{O})

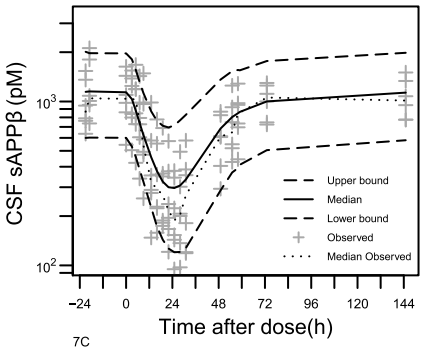

(C) sAPPβ

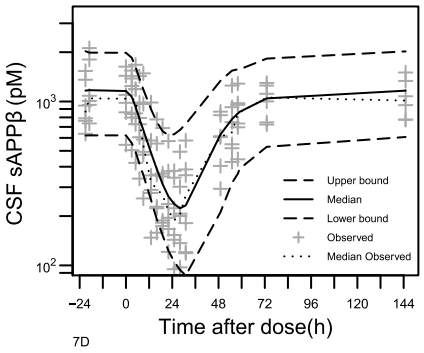

(D) sAPPβ (With Aβ_{O})

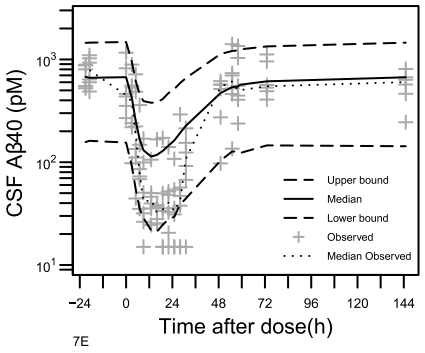

(E) Aβ40

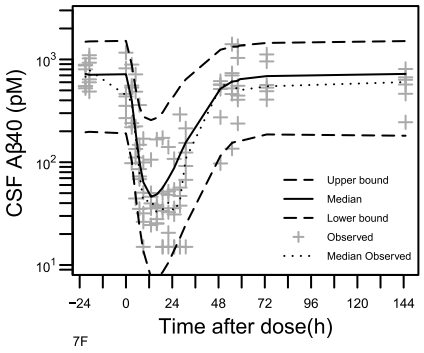

(F) Aβ40 (With Aβ_{O})

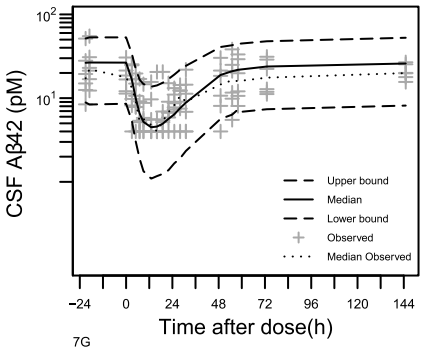

(G) Aβ42

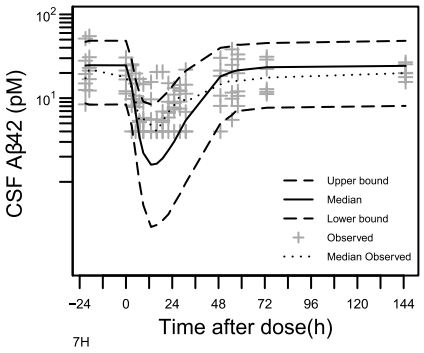

(H) Aβ42 (With Aβ_{O})

Downloaded from jpet.aspetjournals.org at ASPET Journals on April 10, 2024